Nondegenerate two-photon absorption in zinc blende semiconductors

D. C. Hutchings* and E. W. Van Stryland

Center for Research in Electro-Optics and Lasers, University of Central Florida, Orlando, Florida 32826

Received April 10, 1992; revised manuscript received June 16, 1992

An algorithm is presented for the calculation of the nondegenerate two-photon absorption coefficient by using second-order perturbation theory and a Kane band-structure model, including the effects of nonparabolicity and nonzone-center wave functions. The polarization dependence is included by correctly accounting for the symmetry of the electronic wave functions. A comparison is made with degenerate two-photon absorption data in various zinc blende semiconductors, and excellent agreement is found without the use of fitting parameters. Comparisons are also made with nondegenerate two-photon absorption spectra measured in ZnSe and ZnS by using a picosecond continuum and with some polarization-dependent measurements obtained by a two-color Z-scan measurement.

INTRODUCTION

Degenerate (self-action) two-photon absorption (2PA) in a zinc blende semiconductor was previously described and characterized; see, e.g., Refs. 1–3. However, there has been recent interest in the nondegenerate 2PA whereby one light field induces absorption in a second light field, resulting in the loss of one photon from each field. Here we use the term nondegenerate to indicate the effect of one light beam on a different (usually in wavelength or polarization) light beam (cross action), as opposed to self-action effects, which are the effects of light beams on themselves and which we term degenerate. This interest is due partly to recent measurements of nondegenerate nonlinear absorption in semiconductors[4,5] but also to the fact that the nondegenerate absorption can be used to determine the nonresonant nonlinear refractive index n_2 by means of a nonlinear Kramers–Kronig relation.[6,7]

A calculation for degenerate 2PA that uses a two-parabolic-band model for a semiconductor is presented in Refs. 7 and 8. This two-parabolic-band model provides the proper scaling of 2PA with material parameters and gives a frequency dependence matching that of experimental data. However, the absolute value of the predicted values is consistently low by approximately a factor of 2 over a wide range of direct-gap semiconductors and some dielectrics.[3] This factor can be accounted for by using the present band structure, which is more realistic near the center of the Brillouin zone. In particular, the degeneracy of the valence bands and the band nonparabolicity are correctly accounted for. By this improvement in the band-structure model, one can accurately predict 2PA without the use of fitting parameters.

Another reason for using a more comprehensive band-structure model is that the simple two-band model does not, by itself, give any polarization dependence. This is because the two-parabolic-band model does not provide a direction for the momentum matrix element (although most calculations assume a momentum matrix element parallel to the electronic $\mathbf{k}$ vector). The Kane band structure used here automatically provides a direction and a magnitude for the momentum matrix element, permitting the determination of nondegenerate 2PA for arbitrary polarization orientations between the two light inputs. However, as the Kane band structure for zinc blende (cubic) semiconductors is isotropic, there will be no polarization dependence with respect to the crystal orientation.

THEORY OF DEGENERATE TWO-PHOTON ABSORPTION

There have been two basic approaches to the calculation of degenerate 2PA coefficients in a crystalline solid. First, second-order perturbation theory can be used to calculate the transition rate from valence to conduction band (resulting from the absorption of two photons). Second, first-order perturbation theory can be used with electronic wave functions that have been dressed to include the acceleration of the electrons as a result of the ac light field. The latter approach was developed by Keldysh[9] and is often termed tunneling theory.

Second-Order Perturbative Approach

Fermi's golden rule (derived from second-order time-dependent perturbation theory) provides the form of the two-photon transition rate:

$$W_2 = \frac{2\pi}{\hbar}\sum_{vc}\left|\sum_i \frac{\langle\psi_c|\hat{H}_{opt}|\psi_i\rangle\langle\psi_i|\hat{H}_{opt}|\psi_v\rangle}{E_{iv}(\mathbf{k})-\hbar\omega}\right|^2 \delta(E_{cv}(\mathbf{k})-2\hbar\omega), \tag{1}$$

where $\hat{H}_{opt} = (e/mc)\mathbf{A}\cdot\hat{\mathbf{p}}$ is the optical interaction Hamiltonian applicable to solids, $\psi_c(\psi_v)$ is the Bloch wave function for the conduction (valence) band, and $E_{cv}(\mathbf{k})$ is the energy difference between the bands. The sum is over all possible intermediate states i and over all possible transitions starting from a filled state and ending at an empty state (usually valence to conduction band for an intrinsic semiconductor), i.e., a sum over bands and the electronic wave vector $\mathbf{k}$. The subtlety in this calculation is in de-

0740-3224/92/112065-10$05.00

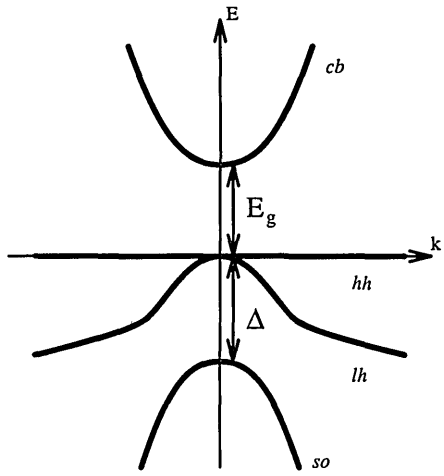

Fig. 1. Band structure for a zinc blende semiconductor near the center of the Brillouin zone as given by Kane.[12] Only the set of four doubly degenerate (in spin) bands are considered: conduction band (cb), heavy-hole band (hh), light-hole band (lh), and split-off band (so).

ciding what model to choose for the band structure and over what bands the summations will be performed.

The simplest model for a semiconductor consists of a single parabolic conduction band and a single parabolic valence band in which the intermediate states are also these bands.[8,10] Hence the summation will involve an interband (allowed) and an intraband (forbidden) matrix element. This calculation gives a two-photon absorption coefficient of the form

$$\beta(\omega) = K_{\mathrm{pb}} \frac{\sqrt{E_p}}{n_0^2(\omega) E_g^3} F_2\left(\frac{\hbar\omega}{E_g}\right),$$
$$F_2 = \frac{(2x-1)^{3/2}}{(2x)^5}, \qquad (2)$$

where E_p is related to the interband momentum matrix element and for the two-parabolic-band model is defined $E_p = 2|\mathbf{p}_{\mathrm{vc}}|^2/m_0$ (E_p is approximately 21 eV for most semiconductors),[11] n_0 is the linear refractive index, and E_g is the band gap. K_{pb} is a material independent constant, which the two-band theory gives as[7]

$$K_{\mathrm{pb}} = \frac{2^9\pi}{5} \frac{e^4}{\sqrt{m_0 c^2}} = 1940 \text{ cm/GW (eV)}^{5/2}. \qquad (3)$$

Equation (3) gives the correct material scaling ($n_0^{-2}E_g^{-3}$) over a large range of semiconductors and wide-gap optical materials[3]; however, 2PA coefficient predictions are consistently low. This difference has been compensated for by fitting the constant K_{pb} to the experimental data, which gives a value for the constant of $K_{\mathrm{pb}} = 3100$ in the same units as above.[3]

One of the deficiencies of the above model is that it does not correctly account for the valence band degeneracy. Zinc blende semiconductors usually have a valence band maximum at the center of the Brillouin zone. This maximum consists of three bands: a heavy-hole band and a light-hole band (degenerate at $k = 0$) with a spin–orbit split-off band separated by the spin–orbit interaction energy Δ (Fig. 1). For direct gap materials (conduction band minimum also at zone center) the theory of Kane[11,12] provides a good description of the bands and the Bloch wave functions around zone center, which is sufficient for many of the band-edge optical properties.

Lee and Fan[13] used the Kane band structure with parabolic bands to determine 2PA coefficients (they also discussed excitonic effects). Two-photon transitions still consist of an allowed and a forbidden transition from a valence to a conduction band, but now possible forbidden transitions consist of intervalence band transitions as well as the self-transitions that exist for the two-band model. This calculation (neglecting the split-off band, i.e., $\Delta \gg E_g$, and without excitonic contributions) results in a 2PA coefficient that is a factor of 2.7 greater than that obtained from the two-parabolic-band model but with identical frequency and material dependencies. This form of calculation was extended by Pidgeon *et al.*,[14] who included nonparabolicity, and by Weiler,[2] who correctly accounted for nonzone-center wave functions with nonparabolicity, which results in a significant reduction in the expected 2PA coefficient. The latter calculation gives a predicted 2PA coefficient that agrees well with (reliable) experimental data for a wide range of semiconductors and optical solids.[3,15]

Tunneling Approach

Keldysh's tunneling theory involves the use of dressed electronic wave functions, which include the effect of an ac electric field and first-order perturbation theory. It not only provides 2PA coefficients but can be used for any multiphoton process. Jones and Reiss applied this method to a two-parabolic-band model of a semiconductor, using an S-matrix approach, for circularly polarized light,[16] and Brandi and de Araújo made a similar application for linearly polarized light.[17] Provided that the same band-structure assumptions are used in both cases, exactly the same result as that predicted by second-order perturbation theory is obtained for 2PA. This is not surprising since the dressed-electron-states approach is equivalent to a self-transition (intraband) in the second-order perturbation theory approach. However, the tunneling theory cannot easily be applied to the Kane band structure, as the tunneling approach has problems dealing with multiple valence band degeneracies and so cannot correctly account for intervalence band transitions. Care needs to be taken when one is using tunneling theory for mulitphoton absorption in general, as this theory often does not account for the dominant contributions. For example, in three-photon absorption the dominant term arises from a threefold interband transition,[8] whereas tunneling theory accounts only for terms corresponding to one interband and two intraband transitions, which are usually much less significant.

To conclude this preliminary discussion on degenerate 2PA theory, a simple two-parabolic-band model of a semiconductor (that uses either the second-order perturbative or the tunneling approach) provides the material scaling and general frequency dependence but usually underestimates β by approximately a factor of 2 (this difference has been compensated for by fitting to measured data). Including other factors, such as correct valence band degeneracies, nonparabolicity, and correct electronic wave functions away from zone center, in the calculation provides an accurate prediction of the degenerate β without the use of fitting parameters.

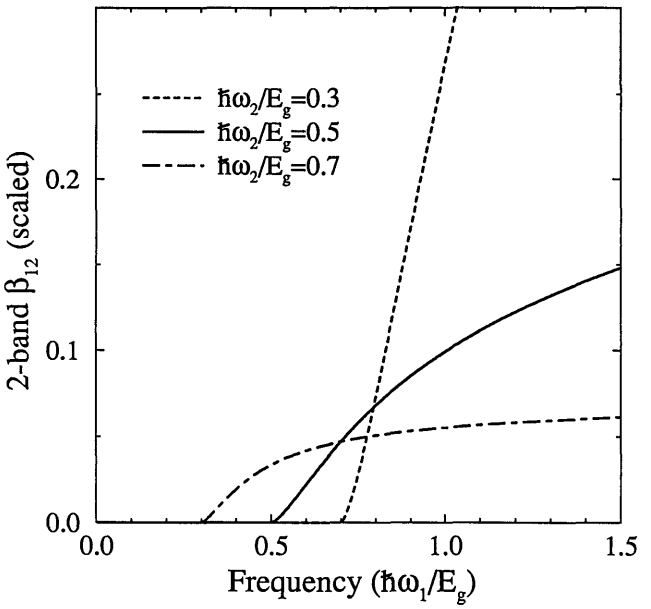

Fig. 2. Theoretical frequency dependence of the nondegenerate 2PA for three different pump frequencies, $\hbar\omega_2 = 0.3, 0.5, 0.7$ for a two-parabolic-band model.

THEORY OF NONDEGENERATE TWO-PHOTON ABSORPTION

In the presence of 2PA alone (i.e., with no linear absorption), the absorption of two spatially and temporally overlapping light beams is described with the following coupled set of equations showing both degenerate (β_{ii}) and nondegenerate (β_{ij}) terms:

$$\frac{\partial I_1}{\partial z} = -\beta_{11} I_1^2 - 2\beta_{12} I_1 I_2,$$

$$\frac{\partial I_2}{\partial z} = -\beta_{22} I_2^2 - 2\beta_{21} I_1 I_2. \tag{4}$$

The factor of 2 in the nondegenerate term is sometimes referred to as weak-wave retardation,[18] and this definition ensures that the nondegenerate coefficient approaches the degenerate one as the parameters of the I_2 beam approach that of I_1, i.e., $\beta_{12} \to \beta_{11}$ as $\omega_2 \to \omega_1$.

Two-Parabolic-Band Model

The nondegenerate 2PA coefficient can be determined by using two parabolic bands and an S-matrix (tunneling) approach[7] or second-order perturbation theory to give

$$\beta_{12} = K_{\mathrm{pb}} \frac{\sqrt{E_p}}{n_0(\omega_1) n_0(\omega_2) E_g^3} F_2^{\mathrm{nd}}\left(\frac{\hbar\omega_1}{E_g}; \frac{\hbar\omega_2}{E_g}\right), \tag{5}$$

where the spectral function F_2^{nd} is defined as

$$F_2^{\mathrm{nd}}(x_1; x_2) = \frac{(x_1 + x_2 - 1)^{3/2}}{2^7 x_1 x_2^2}\left(\frac{1}{x_1} + \frac{1}{x_2}\right)^2, \tag{6}$$

provided $x_1 + x_2 > 1$, and is zero otherwise. For the two-parabolic-band model we define the parameter $E_p = 2|\mathbf{p}_{vc}|^2/m_0$. The functional form of F_2^{nd} is shown in Fig. 2.

Kane Band-Structure Model

In a manner similar to our treatment of the degenerate case, we now use a more realistic band structure for the determination of the relevant optical transitions close to the center of the Brillouin zone. The model used in the following calculation was developed by Kane[11,12] and is based on $\mathbf{k} \cdot \mathbf{p}$ theory with spin–orbit interaction for three-valence bands plus one conduction band. The basis functions are denoted $S\uparrow$ and $S\downarrow$ for the two spin states for the unperturbed conduction band with spherical symmetry and $X\uparrow$, $X\downarrow$, $Y\uparrow$, $Y\downarrow$, $Z\uparrow$, and $Z\downarrow$ with p-like symmetry for the unperturbed valence bands. The resulting band structure is shown in Fig. 1 and consists of a conduction band (cb), heavy-hole (hh) and light-hole (lh) valence bands degenerate at $k = 0$, and a split-off (so) valence band removed by an energy Δ at $k = 0$. On diagonalization, the band energies can be obtained from

$$E' = 0,$$

$$E'(E' - E_g)(E' + \Delta) - (kP)^2(E' + 2\Delta/3) = 0, \tag{7}$$

where $E' = E - (\hbar^2/2m_0)k^2$ is the electron energy with the free-electron mass taken into account and P is the Kane parameter defined from the momentum matrix element:

$$P = -\frac{i\hbar}{m_0}\langle S|p_x|X\rangle = -\frac{i\hbar}{m_0}\langle S|p_y|Y\rangle = -\frac{i\hbar}{m_0}\langle S|p_z|Z\rangle. \tag{8}$$

The first of Eqs. (7) gives the heavy-hole energies, which are zero (plus the free-electron mass contribution) because there is no coupling with other bands, and the cubic equation provides the energies for the conduction, light-hole valence, and split-off valence bands. This diagonalization is such that the total angular momentum (sum of orbital plus spin) $\boldsymbol{J} = \boldsymbol{L} + \boldsymbol{\sigma}$ and its z projection J_z are also diagonal in the new basis. The conduction band ($L = 0, \sigma = 1/2$) has the two (degenerate) spin states of $J = 1/2$, with $J_z = \pm 1/2$. The valence bands ($L = 1, \sigma = 1/2$) have the possible values of $J = 3/2$, $J_z = \pm(3/2)$ for the heavy-hole band, or $J = 3/2$, $J_z = \pm(1/2)$ for the light-hole band, and of $J = 1/2$, $J_z = \pm(1/2)$ for the split-off band. The diagonalization also gives the electronic wave functions

$$\begin{aligned}
\phi_{i\alpha} &= a_i(iS\downarrow) + b_i[(X - iY)\uparrow/\sqrt{2}] + c_i(Z\downarrow),\\
\phi_{i\beta} &= a_i(iS\uparrow) + b_i[-(X + iY)\downarrow/\sqrt{2}] + c_i(Z\uparrow),\\
\phi_{\mathrm{hh}\alpha} &= [(X + iY)\uparrow/\sqrt{2}],\\
\phi_{\mathrm{hh}\beta} &= [(X - iY)\downarrow/\sqrt{2}],
\end{aligned} \tag{9}$$

where α and β denote the two (degenerate) spin states and the coefficients for the conduction, light-hole, and split-off bands are determined from the energies

$$\begin{aligned}
a_i &= kP(E_i' + 2\Delta/3)/N,\\
b_i &= (\sqrt{2}\Delta/3)(E_i' - E_g)/N,\\
c_i &= (E_i' - E_g)(E_i' + 2\Delta/3)/N,
\end{aligned} \tag{10}$$

where $N = (a_i^2 + b_i^2 + c_i^2)^{1/2}$ is a normalizing factor.

The transition rate for nondegenerate 2PA can be determined by using second-order perturbation theory[13]:

$$W_2^{\mathrm{nd}} = \frac{2\pi}{\hbar}\sum_{\mathrm{vc}}\left|\sum_i\left[\frac{\langle c|\hat{H}_2|i\rangle\langle i|\hat{H}_1|v\rangle}{E_{iv}(\mathbf{k}) - \hbar\omega_1} + \frac{\langle c|\hat{H}_1|i\rangle\langle i|\hat{H}_2|v\rangle}{E_{iv}(\mathbf{k}) - \hbar\omega_2}\right]\right|^2 \times \delta[E_{\mathrm{cv}}(\mathbf{k}) - \hbar\omega_1 - \hbar\omega_2], \tag{11}$$

Table 1. z Components of the Scaled Momentum Matrix Element $M_{ij} = \langle i|p_z|j\rangle\hbar/m_0P$ as a Function of the Electronic k Vector in Polar Coordinates[a]

Spin States	c α	hh α	lh α	so α
c α	$2a_cc_s\cos\theta$	0	$(a_cc_l + a_lc_c)\cos\theta$	$(a_cc_s + a_sc_c)\cos\theta$
c β	0	$-\frac{a_c}{\sqrt{2}}\sin\theta$	$-\frac{(a_cb_l - a_lb_c)}{\sqrt{2}}\sin\theta$	$-\frac{(a_cb_s - a_sb_c)}{\sqrt{2}}\sin\theta$
hh α	0	0	0	0
hh β	$-\frac{a_c}{\sqrt{2}}\sin\theta$	0	$-\frac{a_l}{\sqrt{2}}\sin\theta$	$-\frac{a_s}{\sqrt{2}}\sin\theta$
lh α	$(a_cc_l + a_lc_c)\cos\theta$	0	$2a_lc_l\cos\theta$	$(a_lc_s + a_sc_l)\cos\theta$
lh β	$\frac{(a_cb_l - a_lb_c)}{\sqrt{2}}\sin\theta$	$-\frac{a_l}{\sqrt{2}}\sin\theta$	0	$-\frac{(a_lb_s - a_sb_l)}{\sqrt{2}}\sin\theta$
so α	$(a_cc_s + a_sc_c)\cos\theta$	0	$(a_lc_s + a_sc_l)\cos\theta$	$2a_sc_s\cos\theta$
so β	$\frac{(a_cb_s - a_sb_c)}{\sqrt{2}}\sin\theta$	$-\frac{a_s}{\sqrt{2}}\sin\theta$	$\frac{(a_lb_s - a_sb_l)}{\sqrt{2}}\sin\theta$	0

[a]The labels α and β refer to the two (degenerate) spin states in each band [conduction (c), heavy-hole (hh), light-hole (lh), and split-off (so)]. The coefficients a_i, b_i, and c_i are the Kane coefficients determined from Eqs. (10). Only transitions from α spin states are shown here, but to get transitions from the β spin states the relations $M_{i\beta,j\beta} = M_{i\alpha,j\alpha}$ and $M_{i\alpha,j\beta} = M^*_{j\beta,i\alpha}$ can be used.

where the interaction Hamiltonians are given by

$$\hat{H}_j = \frac{e}{m_0c}\mathbf{A}_j\cdot\hat{\mathbf{p}},$$
$$= \frac{e}{im_0\omega_j}\left[\frac{2\pi I_j}{n_0(\omega_j)c}\right]^{1/2}\hat{a}_j\cdot\hat{\mathbf{p}}. \quad (12)$$

Here $\hat{a}_j$ is the unit vector in the direction of polarization of the jth optical beam, which has frequency ω_j and an irradiance I_j.

In order to determine this transition rate, one must obtain the momentum matrix element among the various bands described by the Kane theory. Table 1 shows the z component of the scaled momentum matrix element taken among the various sets of bands, which we define as

$$M_{ij}^{(n)}(\mathbf{k}) = \frac{\hbar}{m_0P}\hat{a}_n\cdot\langle j,\mathbf{k}|\hat{\mathbf{p}}|i,\mathbf{k}\rangle. \quad (13)$$

Only the matrix elements from the α spin states are shown, but those from the β spin states can easily be obtained by using the facts that

$$M_{i\beta,j\beta} = M_{i\alpha,j\alpha},$$
$$M_{i\alpha,j\beta} = M^*_{j\beta,i\alpha}. \quad (14)$$

Lee and Fan[13] show a similar table for the particular case of parabolic bands and zone-center wave functions. Here the $\mathbf{k}$ vector is given in polar coordinates (k,θ,ϕ), and the (a,b,c) coefficients are the k-dependent wave function coefficients described in Eqs. (10). For parallel optical polarizations we can take both polarizations to be in the z direction. For arbitrary polarizations we can use the z component for one beam and determine the other matrix element for the appropriate orientation. In examples below we consider cross-polarized beams, so the x component (or the y component) of the momentum matrix element is also required, which we show in Table 2 (using the same formalism as above). Whereas the z component is independent of the ϕ component of the electronic wave vector $\mathbf{k}$, it can be seen the same is not true for the x component.

Using the expression for the nondegenerate two-photon transition rate given in Eq. (11), we obtain the following expression for the 2PA coefficient:

$$\beta_{12}(\omega_1;\omega_2) = \left(\frac{e^2}{\hbar c}\right)^2\frac{\hbar P}{2n_0(\omega_1)n_0(\omega_2){E_g}^3}f_2\left(\frac{\hbar\omega_1}{E_g};\frac{\hbar\omega_2}{E_g}\right),$$
$$= K\frac{\sqrt{E_p}}{n_0(\omega_1)n_0(\omega_2){E_g}^3}f_2\left(\frac{\hbar\omega_1}{E_g};\frac{\hbar\omega_2}{E_g}\right), \quad (15)$$

where the dimensionless spectral function f_2 is defined as

$$f_2(x_1;x_2) = \frac{1}{x_1{x_2}^2}\sum_{vc}\int_0^{2\pi}d\phi\int_0^{\pi}\sin\theta d\theta\int_0^{\infty}\left(\frac{kP}{E_g}\right)^2\frac{d(kP)}{E_g}$$
$$\times\left|\sum_i\left[\frac{M_{ci}^{(2)}M_{iv}^{(1)}}{E_{iv}(k)/E_g - x_1} + \frac{M_{ci}^{(1)}M_{iv}^{(2)}}{E_{iv}(k)/E_g - x_2}\right]\right|^2$$
$$\times\delta\left[\frac{E_{cv}(k)}{E_g} - x_1 - x_2\right]. \quad (16)$$

The material dependent constant K is given by

$$K = \left(\frac{e^2}{\hbar c}\right)^2\frac{\hbar^2}{2\sqrt{2m_0}}, \quad (17)$$

which has the value of 2.2 cm/GW $(\text{eV})^{5/2}$ (allowing E_p and E_g to be given in electron volts), and E_p is related to the Kane parameter P by $E_p = 2m_0P^2/\hbar^2$.

In the Kane band-structure case, there is a dependence on the ratio of the split-off energy to the band gap, Δ/E_g, which is contained within the dimensionless spectral function f_2 (the parameter P also appears, but only for scaling the integral), which obviously does not appear in the two-parabolic-band model. The summations involved are over all valence to conduction band routes via all possible intermediate states (which are themselves the various valence and conduction bands described in this band-structure model). In this calculation only the bands described above are used, i.e., one conduction and three valence bands, each doubly degenerate in spin. Higher band contributions are neglected. With the matrix elements described above for the Kane model, there are 46

Table 2. x Components of the Scaled Momentum Matrix Element $M_{ij} = \langle i|p_x|j\rangle\hbar/m_0P$ as a Function of the Electronic k Vector in Polar Coordinates[a]

Spin States	c α	hh α	lh α	so α
c α	$2a_cc_c \sin\theta\cos\phi$	0	$(a_cc_l + a_lc_c)\sin\theta\cos\phi$	$(a_cc_s + a_sc_c)\sin\theta\cos\phi$
c β	0	$\frac{a_c}{\sqrt{2}}(\cos\theta\cos\phi - i\sin\phi)$	$\frac{(a_cb_l - a_lb_c)}{\sqrt{2}}(\cos\theta\cos\phi + i\sin\phi)$	$\frac{(a_cb_s - a_sb_c)}{\sqrt{2}}(\cos\theta\cos\phi + i\sin\phi)$
hh α	0	0	0	0
hh β	$\frac{a_c}{\sqrt{2}}(\cos\theta\cos\phi - i\sin\phi)$	0	$\frac{a_l}{\sqrt{2}}(\cos\theta\cos\phi - i\sin\phi)$	$\frac{a_s}{\sqrt{2}}(\cos\theta\cos\phi - i\sin\phi)$
lh α	$(a_cc_l + a_lc_c)\sin\theta\cos\phi$	0	$2a_lc_l \sin\theta\cos\phi$	$(a_lc_s + a_sc_l)\sin\theta\cos\phi$
lh β	$-\frac{(a_cb_l - a_lb_c)}{\sqrt{2}}(\cos\theta\cos\phi + i\sin\phi)$	$\frac{a_l}{\sqrt{2}}(\cos\theta\cos\phi - i\sin\phi)$	0	$\frac{(a_lb_s - a_sb_l)}{\sqrt{2}}(\cos\theta\cos\phi + i\sin\phi)$
so α	$(a_cc_s + a_sc_c)\sin\theta\cos\phi$	0	$(a_lc_s + a_sc_l)\sin\theta\cos\phi$	$2a_sc_s \sin\theta\cos\phi$
so β	$-\frac{(a_cb_s - a_sb_c)}{\sqrt{2}}(\cos\theta\cos\phi + i\sin\phi)$	$\frac{a_s}{\sqrt{2}}(\cos\theta\cos\phi - i\sin\phi)$	$-\frac{(a_lb_s - a_sb_l)}{\sqrt{2}}(\cos\theta\cos\phi + i\sin\phi)$	0

[a]Again only transitions from α spin states are shown, and the relations $M_{i\beta,j\beta} = M_{i\alpha,j\alpha}$ and $M_{i\alpha,j\beta} = M^*_{j\beta,i\alpha}$ should be used for the transitions from the β spin states. Abbreviations are defined as for Table 1.

contributing transitions from valence to conduction band, compared with 4 for the two-parabolic-band model (which can be further reduced to one calculation, as all 4 transitions occur at the same magnitude of the **k** vector). In both the two-parabolic-band and the Kane band models, these transitions consist of an allowed term (valence to conduction band) and a forbidden term, i.e., not allowed at $k = 0$ (self-valence, self-conduction, or intervalence band).

The algorithm for computing the nondegenerate 2PA is as follows. First, for the given optical frequencies ω_1 and ω_2, the magnitude of k at which this optical transition occurs is determined. This involves calculating the root of the argument of the Dirac delta function in Eq. (16) [which in turn involves computing the roots of Eqs. (7)]. Second, the wave functions for these states are determined by computing the (a, b, c) coefficients [Eqs. (10)]. Third, the appropriate scaled momentum matrix elements $M_{ij}^{(n)}$ (k dependent) are determined (Tables 1 and 2). Fourth, the summation is performed over all valid intermediate states, and the integrals are computed over the angular coordinates of the **k** wave vector (θ, ϕ).

RESULTS

Indium Antimonide

To check the above algorithm, we first make a comparison with established theories for degenerate 2PA in narrow-gap semiconductors, citing InSb as an example. Weiler[2] gives an analytic expression for the degenerate spectral function f_2 that includes nonparabolicity and nonzone-center wave functions in the limit of a large split-off energy, $\Delta \gg kP, E_g$, which is applicable to narrow-gap semiconductors:

$$f_2^{\mathrm{np}}(x) = \frac{8\pi(2x-1)^{3/2}}{3x^3} \times \left[\frac{4(3x)^{1/2}}{(3x-1)^2} + \left(3x + \frac{3}{2}\right)^{3/2} \frac{(9x^4 + 10x^2 + 6)}{90x^5}\right]. \tag{18}$$

Weiler also gives the correct form of the frequency dependence, using parabolic bands and zone-center wave functions (also in the limit $\Delta \gg kP, E_g$), which was calculated by Lee and Fan[13]:

$$f_2^{\mathrm{pb}}(x) = \frac{8\pi(2x-1)^{3/2}}{\sqrt{6}x^5}\left(4 + \frac{29\sqrt{2}}{12}\right). \tag{19}$$

The material scaling of both of these models is exactly the same as that given above in Eq. (15). These forms are plotted in Fig. 3 for InSb at room temperature (E_g = 0.175 eV; E_p = 21.3 eV; Δ = 0.85 eV), along with the results of the numerical model presented here. It can be seen that the omission of nonparabolicity and nonzone-center wave functions leads to a considerable overestimation of 2PA, except close to the 2PA edge, although the overall shape is qualitatively similar to that in the nonparabolic case. This is a result of the decrease of the interband momentum matrix element with increasing k as the $\mathbf{k} \cdot \mathbf{p}$ perturbation causes more mixing of the s- and p-like wave functions. We find that our calculation gives a result close to that of Weiler's nonparabolic calculation, with only a small deviation at higher photon energies. This deviation is due principally to there being a term proportional to E_g/Δ in the effective mass as a result of the interaction of the split-off band, which is neglected in Weiler's expression. In the same plot we show some experimental data taken with a CO_2 laser at 10.6 and 9.6 μm.[19-22] The spread in the experimental data makes the frequency dependence impossible to confirm, but the results given here seem to confirm that, for 2PA in InSb, nonparabolicity and nonzone-center wave functions have a marked effect on the overall magnitude of the 2PA but that the frequency dependence is not greatly changed, as was stated in Ref. 2.

Degenerate Two-Photon Absorption at 1.06 and 0.53 μm

Reference 3 gives a range of degenerate 2PA measurements in semiconductors at a wavelength of 1.06 μm and its second harmonic, 0.53 μm. The results for the semiconductors with a zinc blende structure are shown in Table 3 along with the predicted values from the present theory. The uncertainty in the measured values was given as ±40%. For CdTe, GaAs, ZnS, and ZnSe, excel-

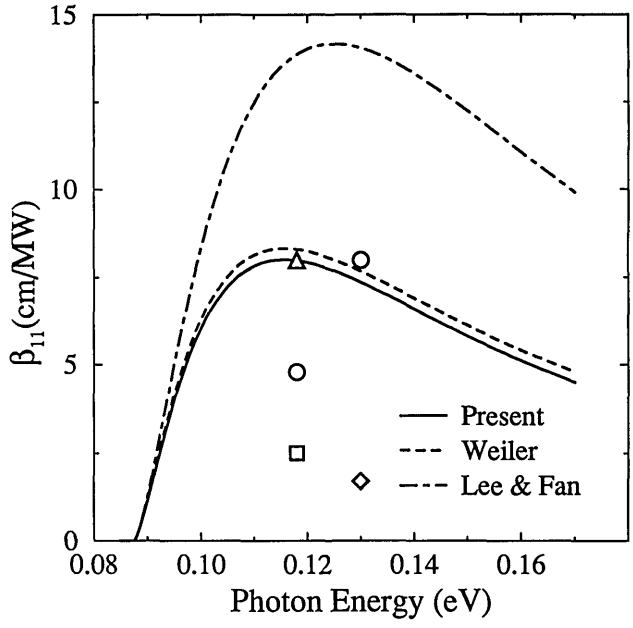

Fig. 3. Frequency dependence of the degenerate 2PA in InSb. Included for comparison are various experimentally determined values at 10.6 and 9.6 μm: △, Ref. 19; ○, Ref. 20; □, Ref. 21; ◇, Ref. 22.

Table 3. Degenerate 2PA in a Variety of Zinc Blende Semiconductors

Material	Wavelength (μm)	β (cm/GW) Ref. 3	Ref. 23	Theoretical[a]
ZnSe	0.532	5.5	5.8	5.0
ZnS	0.532	2.0–3.5	—	3.0
GaAs	1.064	23	26	22
CdTe	1.064	15–22	26	18
ZnTe	1.064	4.5	4.2	1.2

[a]The theoretical values were determined by using the algorithm presented here, which includes band nonparabolicity, the contribution from the split-off band, and the use of nonzone-center wave functions.

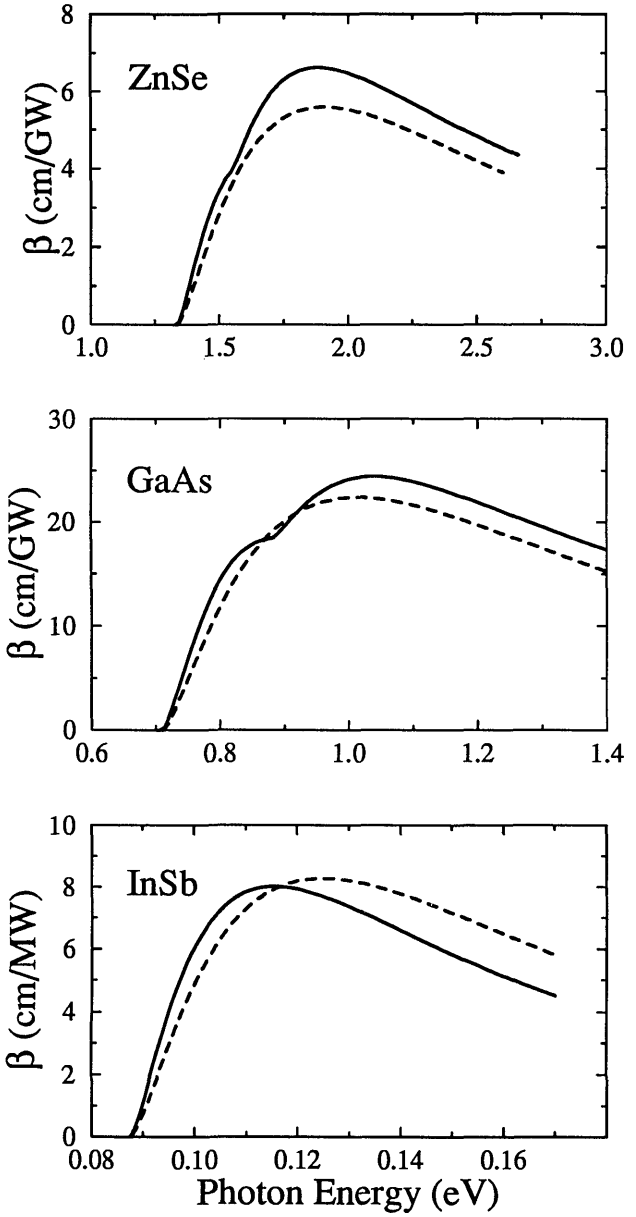

Fig. 4. Comparison of the present calculation (solid curves) with the fitted two-parabolic-band result (dashed curves), i.e., setting $K_{pb} = 3100$ cm/GW $(eV)^{5/2}$, for the degenerate 2PA in InSb, GaAs, and ZnSe.

lent agreement is obtained, especially considering that there are no fitting parameters whatsoever in the present treatment. However, the 2PA in ZnTe at 1.06 μm is considerably underestimated. It should be noted, however, that this measurement lies close to the 2PA edge. It has been suggested that this discrepancy is due to excitonic enhancement since the difference corresponds to only a few times the exciton binding energy.[3] Other possible explanations are that there may be some degree of band tailing or that allowed–allowed transitions via higher bands become relatively more important close to the 2PA edge.

One of the surprising features of the simpler two-parabolic-band model is that, when it is scaled (i.e., $K_{pb} = 3100$), it provides a remarkably good prediction for the degenerate 2PA over a wide range of materials and frequencies.[3] To confirm this fact we compare the results of this model with our present theory in Fig. 4 for InSb, GaAs, and ZnSe. It can be seen that in all three examples the two curves lie fairly close together over the whole frequency range shown here (certainly well within typical experimental errors for these types of measurement). Note, however, that as the band gap increases, the two-parabolic-band result increasingly underestimates β as the split-off band plays a greater role.

Zinc Selenide

One of the semiconductors in which we make a comparison between theory and experiment for the nondegenerate 2PA spectra is ZnSe. In this material the band gap and split-off energies are of comparable magnitudes ($E_g = 2.67$ eV, $E_p = 24.2$ eV, $\Delta = 0.42$ eV), fulfilling neither of Weiler's analytic expressions for the degenerate 2PA that were calculated for $\Delta \gg E_g$ and $\Delta \ll E_g$. That this is so is demonstrated in Fig. 5, which is a plot of the degenerate 2PA coefficient against frequency and from which it can be seen that the exact numerical calculation performed here (solid curve) agrees with Weiler's nonparabolic expression for $\Delta \gg E_g$ (short-dashed curve) close to the 2PA edge but asymptotically approaches the expression for $\Delta \ll E_g$ at higher frequencies. The point of inflection near 1.5 eV in the present calculation occurs because the photon energies have reached the threshold of split-off to conduction band transitions. The data denoted by the circles are two measurements at 0.532 μm,[3,23] which show excellent agreement with the present calculation. Also shown in Fig. 5 is the polarization dependence of the frequency-degenerate 2PA. The solid curve discussed above also gives the nondegenerate 2PA in the limit of identical frequencies and parallel polarizations. The long-and-short-dashed curve shows the same quantity, but now

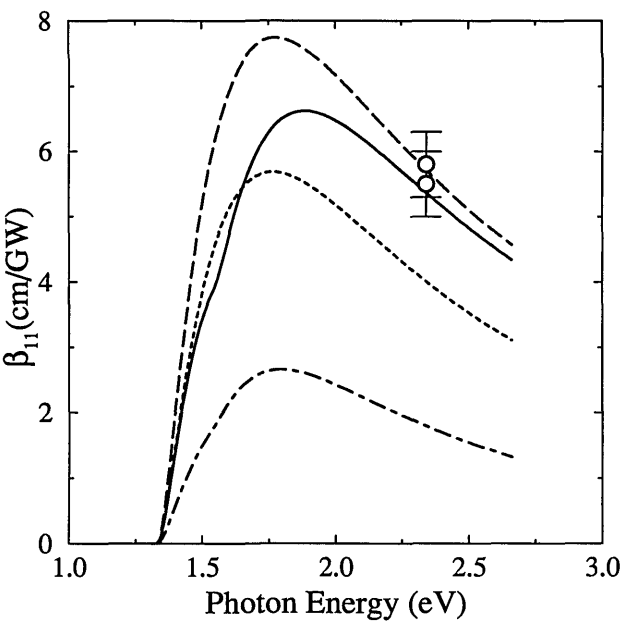

Fig. 5. Frequency dependence of the degenerate 2PA in ZnSe. The solid curve shows the present calculation; the short-dashed curve and the long-dashed curve show Weiler's nonparabolic expressions in the limits $\Delta \gg E_g$ and $\Delta \ll E_g$, respectively. The dotted–dashed curve shows nondegenerate 2PA where the two wavelengths are identical but the optical polarizations are perpendicular. Also included are some data points with appropriate error bars taken from Refs. 3 and 23.

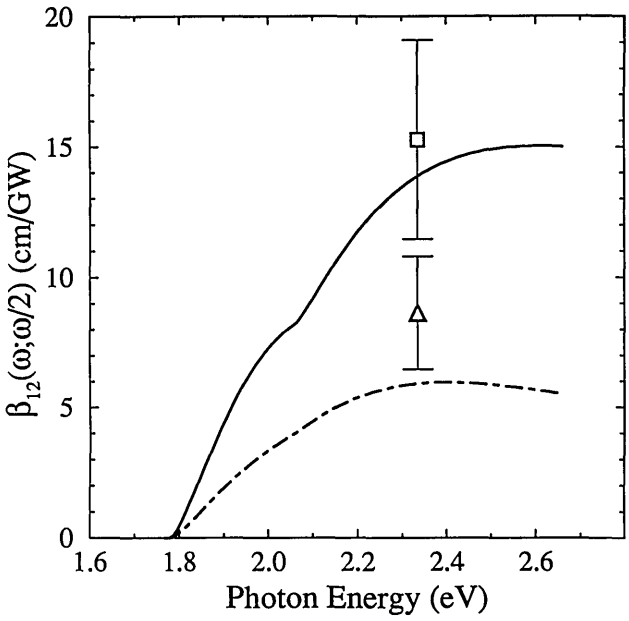

Fig. 6. Nondegenerate 2PA in ZnSe at the second-harmonic frequency that is due to the presence of light at the fundamental frequency. The solid curve corresponds to parallel optical polarizations; the dashed curve; to perpendicular. Two data points are shown, measured at 0.532 μm because of the presence of a beam at 1.064 μm, by the two color Z-scan technique.[5] The square corresponds to parallel polarizations, and the triangle to perpendicular.

the optical polarizations of the two beams are perpendicular. It can be seen that in the perpendicular case the 2PA coefficient is approximately a factor of 2–3 less than in the parallel case over all frequencies beneath the band edge, $\hbar\omega < E_g$. For ZnSe at a wavelength of 705 nm this theory gives a ratio of 2.4 between the two polarization cases, which agrees fairly well with an experimental measurement of 2.[24] Note that the threshold for the split-off transitions is much less obvious in the perpendicular case. This result is a consequence of the direction of the matrix elements involving the split-off band resulting in a reduction in the angular (Euler's) integral for these transitions. It should be noted, though, that one must take care when considering nondegenerate optical effects that arise from two beams of identical frequency, as coherence must play a significant role. The nondegenerate 2PA values given in Fig. 5 should be considered only as the limit obtained, as the two (different) frequencies tend to the same value.

One method of obtaining a nondegenerate 2PA measurement is to frequency double a portion of a pump beam and use it as a probe beam. However, it should be noted that this method can be used only to obtain nondegenerate measurements along a particular line in the (ω_1, ω_2) plane, as the two frequencies used must have a fixed relation between them (i.e., $\omega_1 = 2\omega_2$). Figure 6 shows the nondegenerate 2PA in ZnSe at the second harmonic that is due to the presence of the fundamental within the material, i.e., $\beta(\omega;\omega/2)$. Once again a solid curve is used to denote parallel optical polarizations; and a long-and-short-dashed curve, perpendicular. Again the point of inflection where split-off transitions become allowed is readily seen in the parallel case. The data shown here are nondegenerate 2PA coefficients measured at 0.532 μm that are due to the influence of a strong 1.064-μm pump beam measured by the two-color Z-scan technique.[5]

A recent paper[4] reported the measurement of nondegenerate 2PA in several wide-gap semiconductors by using a pump at 705 nm and a picosecond continuum pulse as a probe. This directly gives the form of nonlinear absorption applicable to the determination of the nonlinear refractive index n_2 by the nonlinear Kramers–Kronig

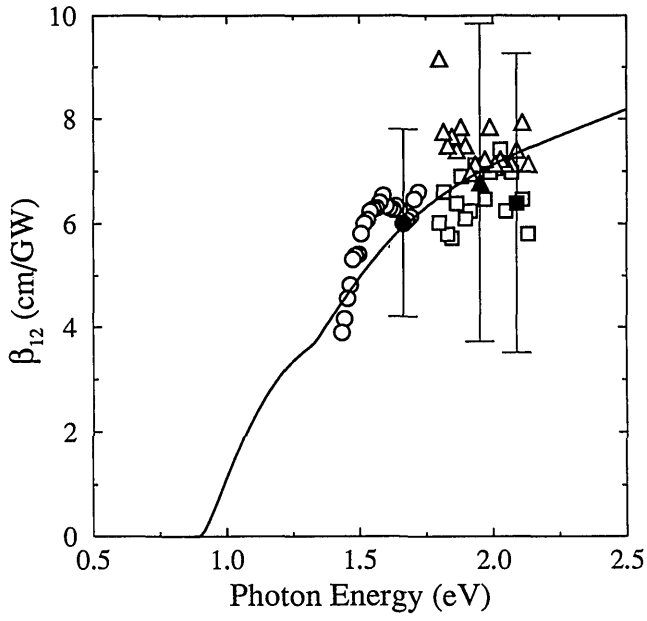

Fig. 7. Nondegenerate 2PA in ZnSe as a function of probe frequency for a fixed pump frequency at 0.705 μm (parallel polarizations). The data are from Ref. 4. The circles correspond to a high irradiance, $I_2 = 8$ GW/cm^2 (errors ±30%), and the squares and triangles to a lower irradiance measurement, $I_2 = 0.7$ GW/cm^2 (errors ±45%).

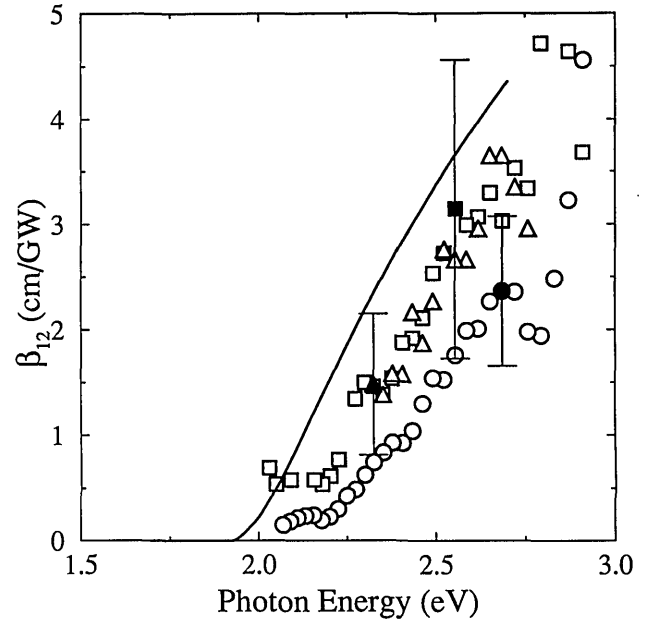

Fig. 8. Nondegenerate 2PA in ZnS as a function of probe frequency for a fixed pump frequency at 0.705 μm (parallel polarizations). The data are from Ref. 4. The circles correspond to a high irradiance, $I_2 = 8$ GW/cm^2 (errors ±30%), the squares to a medium irradiance, $I_2 = 1.8$ GW/cm^2 (errors ±45%), and the triangles to a lower irradiance $I_2 = 0.7$ GW/cm^2 (errors ±45%).

relation.[6] Figure 7 shows the results for ZnSe along with the results of the corresponding theoretical calculation. The circles correspond to a pump irradiance of ≈8 GW/cm^2 and have an estimated error of ±30%. The triangles and the squares correspond to a lower irradiance level (≈0.7 GW/cm^2) and have an estimated error of ±45%. The sizes of these errors make it difficult to infer any details of the nonlinear absorption spectrum, but the magnitude is in complete agreement with the present calculation.

Zinc Sulfide

Reference 4 also presents data for ZnS, which is also a zinc blende semiconductor, but in this case the spin–orbit interaction is small, and the split-off energy is much smaller than the band gap ($E_g = 3.54$ eV, $E_p = 20.4$ eV, $\Delta = 0.064$ eV). In the case of ZnS, the picosecond continuum provided the nondegenerate 2PA around the 2PA edge (i.e., $\hbar\omega_1 + \hbar\omega_2 \sim E_g$), as shown in Fig. 8. Here the circles correspond to an irradiance level of ≈8 GW/cm^2 with an estimated error of ±30%, the squares to ≈8 GW/cm^2 (±45%), and the triangles to ≈0.7 GW/cm^2 (±45%). Once again, the solid curve is the calculated 2PA and shows excellent agreement with the wavelength dependence and magnitude, considering that the calculation is absolute. Note that in this case because of the small split-off energy Δ the point of inflection corresponding to the threshold of split-off transitions is no longer obvious.

CONCLUSIONS

We have presented an algorithm for the determination of 2PA in zinc blende semiconductors. The calculation uses the band structure described by Kane,[11,12] consisting of a conduction band and three valence bands (heavy-hole, light-hole, and split-off) and includes the effects of nonparabolicity and nonzone-center wave functions. The 2PA coefficient is determined from the transition rate, which is calculated by using second-order perturbation theory (Fermi's golden rule).

The motivation for this study is threefold. First, while a simple two-parabolic-band model gives the correct material scaling and spectral dependence, the results of that model have to be scaled to fit reliable experimental data (replacing the material independent constant $K_{pb} = 1940$ with the best-fit value of 3100 for a range of semiconductors[3]). We have shown that this fit provides a good approximation to the fuller band-structure calculation for the degenerate 2PA. However, it is desirable to use a band-structure model that does not require any fitting parameters. The Kane band structure with nonparabolicity and nonzone-center wave functions[2] seems to satisfy this requirement. Second, in order to account for the optical polarization dependence, one must know the direction as well as the magnitude of the momentum matrix element. The simpler two-band model does not provide this, but the polarization dependence is an integral part of the Kane band-structure model. Third, the nondegenerate 2PA is one of the contributions that can be used to determine the nonlinear refractive index n_2 by a nonlinear Kramers–Kronig transformation[6] (the other methods being Raman transitions and the ac Stark effect). This determination has already been made by using a two-parabolic-band model,[17] but again it must be scaled by approximately a factor of 2 to fit the available data. This present research provides the groundwork for a nonlinear Kramers–Kronig calculation of n_2 for the Kane band structure that we hope will not require the use of any fitting parameters.

It is found that the results of the calculation that uses the algorithm presented here agrees well with available degenerate as well as nondegenerate 2PA data in various zinc blende semiconductors (with the exception of degenerate 2PA in ZnTe at 1.06 μm). Previous publications claim that excitonic effects are important even well above the 2PA edge.[2,13] We find that in most of our examples good predictions are obtained without the inclusion of such effects. It is shown in Ref. 25 that the coulombic enhancement for linear absorption vanishes at higher photon energies such that $\hbar\omega - E_g \gg E_b$, where E_b is the exciton binding energy (Rydberg). We would expect the same to be true for nonlinear absorption. The examples given here almost all occur well away from photon energies where coulombic enhancement is relevant (again an exception being 2PA in ZnTe). Also, impurities and defects in the semiconductors will lead to screening of the coulombic potential and band tailing, which will reduce the bound exciton resonant absorption and the unbound contribution that gives rise to the aforementioned enhancement of the 2PA. We conclude that the enhancement reported in Ref. 13 must be considered an upper limit of 2PA.

Another effect that is neglected in the present calculation is any contribution from other bands. This contribution has a twofold effect. First, the calculated band structure will be different when other bands are allowed to mix with the set of four bands used in the band-edge optical properties (conduction plus three valence). For example, these contributions are necessary if one wishes to obtain a heavy-hole effective mass different from that of free electrons. In particular, away from zone center, the calculated shape of the conduction band is quite different from that of the Kane model. So, for instance in ZnSe, significant deviations from the Kane model should occur near 1 eV above the band edge[26] (corresponding to degenerate 2PA 0.5 eV above the 2PA edge). It is quite remarkable that our model (and to a certain extent the two-parabolic-band model) works so well at these higher photon energies. Second, there are possible two-photon transitions for which the additional bands can be used as the intermediate state. However, these transitions should be significant only close to the 2PA edge (as these are allowed–allowed transitions, compared to the allowed–forbidden transitions considered in this paper) and for transitions high into the conduction band (where the energy difference denominators for transitions via a higher band are not so large). For the intermediate photon energies examined here, these extra transitions should be negligible.

We have calculated only the 2PA contribution to the nondegenerate nonlinear absorption, using transition rates that correspond to loss of energy to the material. Loss or even gain from energy transfer between beams (four-wave mixing) is ignored. This is as it should be for 2PA coefficients; however, one must exercise great care in performing experiments in order to separate clearly the loss contributions of 2PA and energy transfer.

ACKNOWLEDGMENTS

The authors thank A. Miller, B. S. Wherrett, M. Sheik-Bahae, and D. J. Hagan for useful discussions; J. Bolger, A. K. Kar, J. R. DeSalvo, and D. J. Hagan for making their data available before publication; and J. Wang for providing additional experimental data used in comparisons here. We gratefully acknowledge the support of the Defense Advanced Research Projects Agency/Center for Night Vision and Electro-Optics and the Florida High Technology and Industry Council.

E. W. Van Stryland is also with the Departments of Physics and Electrical Engineering, University of Central Florida.

*Present address, Department of Electronics and Electrical Engineering, University of Glasgow, Glasgow G12 8QQ, UK.

REFERENCES

1. V. Nathan, A. H. Guenther, and S. S. Mitra, "Review of multiphoton absorption in crystalline solids," J. Opt. Soc. Am. B **2,** 294–316 (1985).
2. M. H. Weiler, "Nonparabolicity and exciton effects in two-photon absorption in zincblende semiconductors," Solid State Commun. **39,** 937–940 (1981).
3. E. W. Van Stryland, H. Vanherzeele, M. A. Woodall, M. J. Soileau, A. L. Smirl, S. Guha, and T. F. Boggess, "Two photon absorption, nonlinear refraction, and optical limiting in semiconductors," Opt. Eng. **24,** 613–623 (1985).
4. J. Bolger, A. K. Kar, B. S. Wherrett, R. DeSalvo, D. C. Hutchings, and D. J. Hagan, "Nondegenerate two-photon absorption spectra of ZnSe, ZnS and ZnO," Opt. Commun. (to be published).
5. M. Sheik-Bahae, J. Wang, J. R. DeSalvo, D. J. Hagan, and E. W. Van Stryland, "Measurement of nondegenerate nonlinearities using a 2-color *Z*-scan," Opt. Lett. **17,** 258–260 (1992).
6. D. C. Hutchings, M. Sheik-Bahae, D. J. Hagan, and E. W. Van Stryland, "Kramers–Kronig relations in nonlinear optics," Opt. Quantum Electron. **24,** 1–30 (1992), tutorial review.
7. M. Sheik-Bahae, D. C. Hutchings, D. J. Hagan, and E. W. Van Stryland, "Dispersion of bound electronic nonlinear refraction in solids," IEEE J. Quantum Electron. **27,** 1296–1309 (1991).
8. B. S. Wherrett, "Scaling rules for multiphoton interband absorption in semiconductors," J. Opt. Soc. Am. B **1,** 67–72 (1984).
9. L. V. Keldysh, "Ionization in the field of a strong electromagnetic wave," Sov. Phys. JETP **20,** 1307–1314 (1965).
10. N. G. Basov, A. Z. Grasyuk, I. G. Zubarev, V. A. Katulin, and O. N. Krokhin, "Semiconductor quantum generator with two-photon optical excitation," Sov. Phys. JETP **23,** 366–371 (1966).
11. E. O. Kane, "Band structure of narrow gap semiconductors," in *Lecture Notes in Physics: Narrow Gap Semiconductors Physics and Applications*, W. Zawadzki, ed. (Springer-Verlag, New York, 1980), Vol. 133, pp. 13–31.
12. E. O. Kane, "Band structure of indium antimonide," J. Phys. Chem. Solids **1,** 249–261 (1957).
13. C. C. Lee and H. Y. Fan, "Two-photon absorption with exciton effect for degenerate bands," Phys. Rev. B **9,** 3502–3516 (1974).
14. C. R. Pidgeon, B. S. Wherrett, A. M. Johnston, J. Dempsey, and A. Miller, "Two-photon absorption in zinc-blende semiconductors," Phys. Rev. Lett. **42,** 1785–1788 (1979).
15. J. H. Bechtel and W. L. Smith, "Two-photon absorption in semiconductors with picosecond laser pulses," Phys. Rev. B **13,** 3515–3522 (1976).
16. H. D. Jones and H. R. Reiss, "Intense-field effects in solids," Phys. Rev. B **16,** 2466–2473 (1977).
17. H. S. Brandi and C. B. de Araújo, "Multiphoton absorption coefficients in solids: a universal curve," J. Phys. C **16,** 5929–5936 (1983).
18. E. W. Van Stryland, A. L. Smirl, T. F. Boggess, M. J. Soileau, B. S. Wherrett, and F. A. Hopf, "Weak-wave retardation and phase-conjugate self-defocusing in Si," in *Picosecond Phenomena III*, Vol. 23 of Chemical Physics, K. B. Eisenthal, R. M. Hochstrasser, W. Kaiser, and A. Laubereau, eds. (Springer-Verlag, Berlin, 1982), pp. 368–371.
19. A. Miller, A. Johnson, J. Dempsey, J. Smith, C. R. Pidgeon, and G. D. Holah, "Two photon absorption in InSb and $Hg_{1-x}Cd_xTe$," J. Phys. C **12,** 4839–4849 (1979).
20. A. M. Johnson, C. R. Pidgeon, and J. Dempsey, "Frequency dependence of two-photon absorption in InSb and HgCdTe," Phys. Rev. B **22,** 825–831 (1980).
21. M. Sheik-Bahae, P. Mukherjee, and H. S. Kwok, "Two-photon and three-photon absorption coefficients in InSb," J. Opt. Soc. Am. B **3,** 379–385 (1986).
22. M. Sheik-Bahae, T. Rossi, and H. S. Kwok, "Frequency dependence of the two-photon absorption coefficient in InSb: tunneling effects," J. Opt. Soc. Am. B **4,** 1964–1969 (1987).
23. A. A. Said, M. Sheik-Bahae, D. J. Hagan, T. H. Wei, J. Wang, J. Young, and E. W. Van Stryland, "Determination of bound and free-carrier nonlinearities in ZnSe, GaAs, CdTe and ZnTe," J. Opt. Soc. Am. B **9,** 405–414 (1992).
24. J. Bolger, Department of Physics, Heriot-Watt University, Riccarton, Edinburgh EH14 4AS, UK (personal communication).
25. R. J. Elliott, "Intensity of optical obsorption by excitons," Phys. Rev. **6,** 1384–1389 (1957).
26. K.-H. Hellwege, ed., *Landolt–Börstein Numerical Data and Functional Relationships in Science and Technology* (Springer-Verlag, Berlin, 1982), Vols. 17a, 17b, Group III.